ACS Chemical Neuroscience

Letter

pubs.acs.org/chemneuro

A Novel Radiotracer for Imaging Monoacylglycerol Lipase in the Brain Using Positron Emission Tomography

Changning Wang,*[,†] Michael S. Placzek,[†,‡] Genevieve C. Van de Bittner,[†] Frederick A. Schroeder,[†] and Jacob M. Hooker[†]

[†]Athinoula A. Martinos Center for Biomedical Imaging, Department of Radiology, Massachusetts General Hospital, Harvard Medical School, Charlestown, Massachusetts 02129, United States

[‡]Department of Psychiatry, McLean Imaging Center, McLean Hospital, Harvard Medical School, Belmont, Massachusetts 02478, United States

ABSTRACT: Monoacylglycerol lipase (MAGL) is a serine hydrolase that hydrolyzes monoacylglycerols to glycerol and fatty acid and plays an important role in neuroinflammation. MAGL inhibitors are a class of molecules with therapeutic potential for human diseases of the central nervous system (CNS), in areas such as pain and inflammation, immunological disorders, and neurological and psychiatric conditions. Development of a noninvasive imaging probe would elucidate the distribution and functional roles of MAGL in the brain and accelerate medical research and drug discovery in this domain. Herein, we describe the synthesis and pilot rodent imaging of a novel MAGL imaging agent, [^{11}C]SAR127303. Our imaging results demonstrate the high specificity, good selectivity, and appropriate kinetics and distribution of [^{11}C]SAR127303, validating its utility for imaging MAGL in the brain. Our findings support the translational potential for human CNS MAGL imaging.

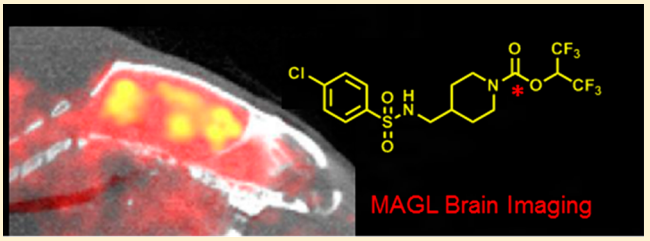

KEYWORDS: *Monoacylglycerol lipase, PET, radiotracer, brain, CNS*

Monoacylglycerol lipase (MAGL) is a serine hydrolase that hydrolyzes monoacylglycerols to glycerol and fatty acid, with highest expression in brain, white adipose tissue, and liver.[1−3] MAGL primarily degrades the endogenous cannabinoid, 2-arachidonoyglycerol (2-AG), one of the two main transmitters of the endogenous cannabinoid system.[1,4,5] Low levels of 2-AG have been observed in pain and inflammation,[6,7] immunological disorders,[8] neurological and psychiatric conditions,[9] obesity and metabolic syndromes,[10,11] and cancer.[12]

In neuroinflammatory regions, MAGL is upregulated to produce less 2-AG.[13−15] Both genetic and pharmacological blockades of MAGL show anti-inflammatory effects in the brain and neuroprotective effects in mouse models of Parkinson's disease and Alzheimer's disease, two examples of profound brain dysfunction involving neuroinflammation.[14,15] In addition, a recent study found that MAGL releases arachidonic acid (AA), the precursor for proinflammatory prostaglandin synthesis in certain tissues. Inhibiting MAGL lowered AA levels in the brain (elevation of 2-AG), which resulted in reduced levels of pro-inflammatory prostaglandin and thromboxane.[14] The importance of MAGL in neuroinflammatory diseases has led to the development of MAGL-selective inhibitors,[1,16,17] such as JZL184 and KML29, which are in the *O*-aryl carbamate class.[13,18] MAGL blockade by JZL184 reduced colonic proinflammatory cytokines in a trinitrobenzenesulfonic acid-induced colitis model resulting in reduced brain inflammation.[19] Currently, it is not possible to interrogate target engagement of MAGL inhibitors in vivo. One result of this is the slowed optimization of small molecule inhibitors for clinical application, including leads from the carbamate class.

Understanding the relationship between MAGL engagement in the brain and inhibitor dosing is essential to advancing the MAGL therapeutic discovery and dose selection process. Molecular imaging, such as positron emission tomography (PET), is an ideal tool to study the drug−target interaction, as it is noninvasive, has exquisite sensitivity and selectivity, and can be translated to human brain imaging. Developing novel MAGL PET imaging probes will significantly accelerate the entire process of investigating MAGL expression and activity in the brain, quickly identifying lead MAGL inhibitors in preclinical and translational research.

However, to our knowledge, no PET radiotracers targeting MAGL have been reported. Although efforts have been made to evaluate several radiolabeled MAGL inhibitors, these compounds lack sufficient brain uptake required for PET brain imaging.[20] Herein, we report a novel MAGL PET radiotracer ([^{11}C]SAR127303), which is based on a highly potent and selective MAGL inhibitor (SAR127303)[4] and demonstrates suitable pharmacokinetic properties in a pilot rodent study.

Special Issue: Neuroinflammation

Received: November 5, 2015
Accepted: December 22, 2015
Published: December 22, 2015

DOI: 10.1021/acschemneuro.5b00293
ACS Chem. Neurosci. 2016, 7, 484−489

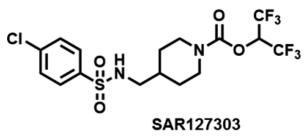

IC_{50} (nM)	3.8 (mouse)	29 (human)
C_{max} [a] (ng/mL)	218 (plasma)	2330 (brain)
MW	tPSA	Log *D*
482.8 g/mol	75.7	1.9

a. P.O. 10 mg/kg

Figure 1. SAR127303 is a highly selective inhibitor of mouse and human MAGL. Griebel et al. reported the pharmacokinetics of SAR127303 recently.[4] Single oral administration (p.o.) of SAR127303 at 10 mg/kg showed high concentration in mouse brain. Plasma and brain C_{max} were observed 4 h after SAR127303 administration.[4]

Scheme 1[a]

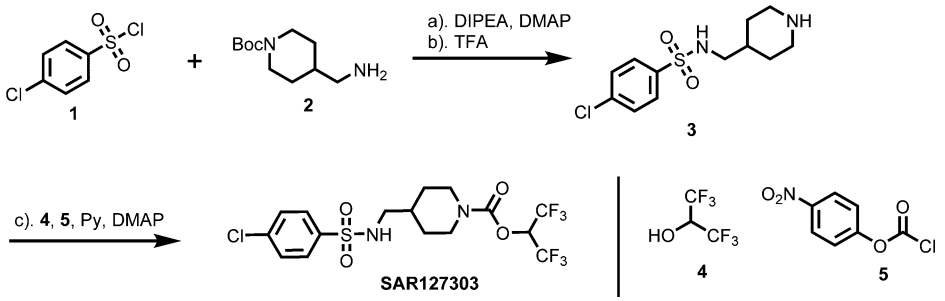

[a]Reagents and conditions: (a) 1 (1.0 equiv), **2** (1.0 equiv), DIPEA (1.5 equiv), DMAP (0.1 equiv), DCM (15 mL), 0 °C to rt, 16 h, 72%; (b), TFA (10 equiv), DCM (2 mL), 0 °C to rt, 16 h, 85%; (c) **4** (1.0 equiv), **5** (2.0 equiv), pyridine (2.0 equiv), DMAP (0.05 equiv), DCM (3 mL), 0 °C to rt, 16 h; then **3** (1.0 equiv), DIPEA (2.5 equiv), DCM (15 mL), 0 °C to rt, 16 h, 8%.

Scheme 2[a]

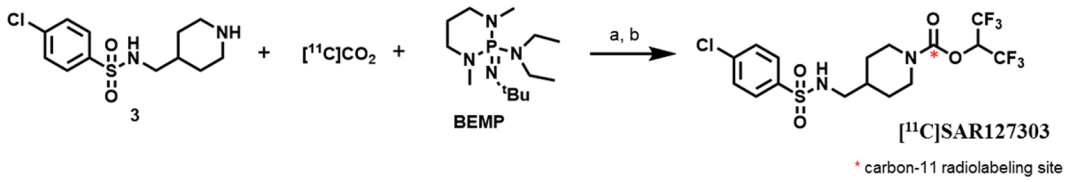

[a][11C]CO_2 fixation reaction forming [11C]SAR127303. a = $POCl_3$, 1 min, rt; b = HFIP, 1 min, rt, then quenched with water and purified by HPLC. Radiochemical yield (RCY): 3−6% based on the trapped [11C]CO_2 (decay uncorrected). Specific activity at time of injection: 1.6−2.3 mCi/nmol.

RESULTS AND DISCUSSION

Physiochemical Properties of SAR127303. A number of major factors determine the success of a radiotracer candidate for imaging MAGL in the brain. The binding affinity and selectivity for MAGL must be high enough to produce sufficient signal for detection. SAR127303 has been recently developed and evaluated by Sanofi.[4] SAR127303 is a highly selective inhibitor of mouse and human MAGL (IC_{50} = 3.8 and 29 nM, respectively).[4] The binding selectivity of SAR127303 was tested on more than 200 targets (receptors, ion channels, enzymes, transporters, and kinases), including cannabinoid receptors (CB1 and CB2) and other human serine hydrolases (e.g., FAAH) at 10 mM. No significant inhibition was observed against these targets, with the exception of α/β-hydrolase 6 (ABHD6, a serine hydrolase for 2-AG hydrolysis).[4] However, MAGL is responsible for approximately 85% of CNS-centered 2-AG hydrolysis[21,22] while ABHD6 only accounts for approximately 4% of brain 2-AG hydrolase activity,[22,23] indicating radiolabeled SAR127303 could be used as a probe for monitoring MAGL-regulated 2-AG hydrolysis.

High brain uptake of the radiotracer is important for imaging MAGL in the brain. The molecular weight, measured log *D*, and total polar surface area (tPSA) of SAR127303 are within the typical range for small molecules that demonstrate good brain penetration (Figure 1). Indeed, the brain to plasma ratio of SAR127303 is above 10 after p.o. administration to male mice at 10 mg/kg.[4] Therefore, SAR127303 is a good probe candidate for radiolabeling and subsequent brain imaging of MAGL with PET.

Synthesis of SAR127303 and the PET Imaging Agent, [11C]SAR127303. To date, most MAGL inhibitors, including SAR127303, are carbamate-based inhibitors that form irreversible, covalent bonds between the carbamoyl moiety and Ser132 of the enzyme's catalytic triad with the expulsion of a leaving group.[24] Therefore, the carbamoyl group is an ideal radiolabeling site. The chemical synthesis of SAR127303 (Scheme 1) and its intermediates were performed by SAI Life Sciences Ltd. Briefly, intermediate **3** was prepared by the coupling reaction with **1** and **2**. Compound **3** was allowed to react with the intermediate formed from **4** and **5** to afford the desired product SAR127303.

To insert the radiolabel at the carbonyl of the carbamate, a one-pot [11C]CO_2 fixation method was employed (Scheme 2),[25] which is a base-catalyzed reaction that forms carbamates from [11C]CO_2. Briefly described, [11C]SAR127303 was synthesized by bubbling cyclotron-produced [11C]CO_2 into a sealed vial with **3** in acetonitrile in the presence of 2-*tert*-butylimino-2- diethylamino-1,3-dimethylperhydro-1,3,2-diazaphosphorine (BEMP).[20] When activity peaked, $POCl_3$ was added and the mixture was stirred for 1 min to form the

DOI: 10.1021/acschemneuro.5b00293
ACS Chem. Neurosci. 2016, 7, 484−489

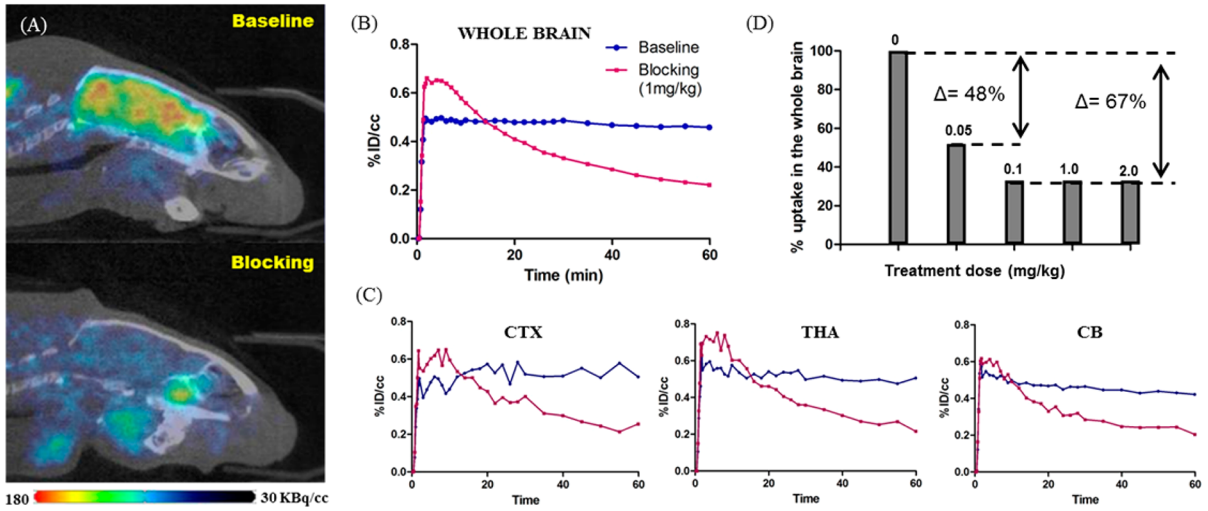

Figure 2. Rodent in vivo PET imaging with [^{11}C]SAR127303 reveals blockable uptake in brain. (A) Summed PET-CT images (30−60 min) following injection with [^{11}C]SAR127303 at baseline or after 5 min pretreatment with 1.0 mg/kg unlabeled SAR127303 (self-blocking). (B) [^{11}C]SAR127303 has high uptake in the whole brain with significant blockade after pretreatment with SAR127303 at 1.0 mg/kg. (C) [^{11}C]SAR127303 shows blockade in brain regions such as cortex (CTX), thalamus (THA), and cerebellum (CB) after pretreatment with SAR127303 at 1.0 mg/kg. (D) SAR127303 pretreatment at 0.05, 0.1, 1.0, and 2.0 mg/kg shows activity blockade in the brain.

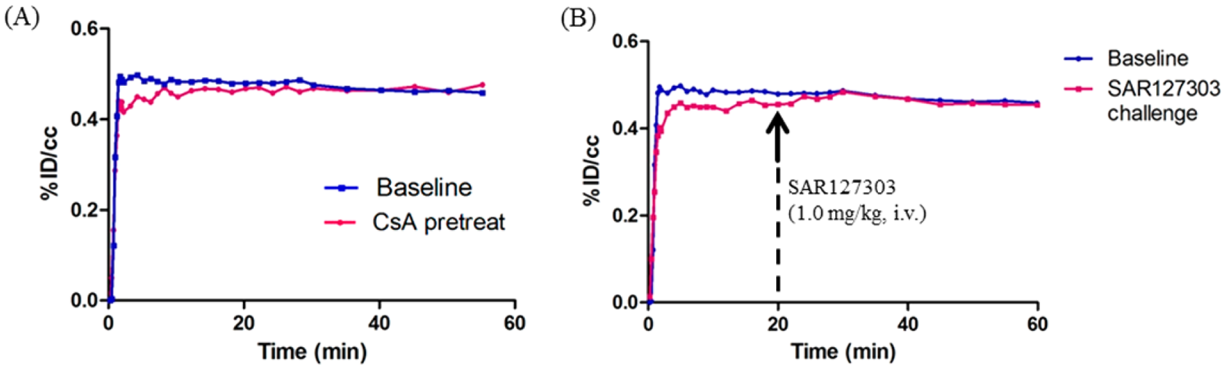

Figure 3. (A) Brain uptake of [^{11}C]SAR127303 in rats is equivalent 30 min after pretreatment with vehicle (control) or the P-glycoprotein (Pgp) inhibitor cyclosporin A (CsA, 25 mg/kg, i.v.). (B) Equilibrium binding of [^{11}C]SAR127303 is undisrupted by administration of unlabeled SAR127303 (1.0 mg/kg, i.v.) 20 min after tracer injection, demonstrating irreversible MAGL binding in the brain.

putative mixed anhydride. Hexafluoroisopropanol (HFIP) was then introduced and the mixture was stirred for 1 min before quenching with water. All radiochemistry was carried out with no heating or cooling, as previously described,[20] and purified by semipreparative HPLC. Radiosynthesis of [^{11}C]SAR127303 was prepared 30−34 min after end of bombardment (EOB) with adequate radiochemical yields (3−6%, nondecay corrected, calculated from initial trapped [^{11}C]CO_2) and final formulation ready for injection with high radiochemical purity (>95%) and good specific activity (1.6−2.3 mCi/nmol at time of injection).

In vivo PET-CT Imaging with [^{11}C]SAR127303 in Rodents. Initial evaluation of [^{11}C]SAR127303 in vivo was conducted in rodents with dynamic brain PET. [^{11}C]-SAR127303 exhibited high BBB penetration and sustained binding over the 60 min scan when administered by intravenous bolus injection (0.2−0.5 mCi (80−310 ng) per animal), as shown in Figure 2. [^{11}C]SAR127303 displayed highest uptake in the cortex, thalamus, and cerebellum. Based on a whole-brain analysis, the concentration of [^{11}C]-SAR127303 in the brain reached a maximum at ∼2 min postinjection.

To investigate the specificity of [^{11}C]SAR127303, we performed PET imaging studies in rats with 5 min i.v. pretreatment of unlabeled SAR127303 at 0.05, 0.1, 1.0, and 2.0 mg/kg. At 0.05 mg/kg, we found a 48% reduction in binding, estimated as the percent change in whole-brain radioactivity between peak uptake at 2 min and the lowest uptake at 60 min (Figure 2). Increasing the dose of unlabeled SAR127303 to 0.1 mg/kg resulted in an ∼67% reduction in [11C]SAR127303 brain uptake, and we observed a similar blockade with 1.0 and 2.0 mg/kg unlabeled SAR127303, indicating saturation at 0.1 mg. This finding demonstrates a high saturability of [^{11}C]SAR127303 for MAGL, with a dose-dependent response to self-blockade and ∼30% of uptake attributed to nonspecific binding.

To support the notion that [^{11}C]SAR127303 was not effluxed from the brain by the P-glycoprotein (P-gp), we measured radioligand uptake in brain after treatment with the P-gp inhibitor, cyclosporin A (CsA) and found no difference compared to control treatment (Figure 3A). Additionally, [^{11}C]SAR127303 binding in rat brain was not disrupted (k_{off} = 0) by i.v. challenge with unlabeled SAR127303 20 min after tracer administration.[26] This provided confirmation of the

DOI: 10.1021/acschemneuro.5b00293
ACS Chem. Neurosci. 2016, 7, 484−489

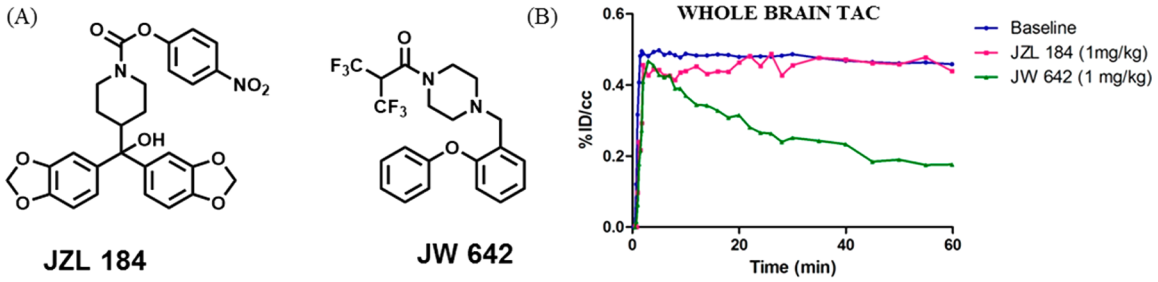

Figure 4. (A) Structures of MAGL selective inhibitors, JZL184 (IC_{50} = 8 nM) and JW642 (IC_{50} = 3.7 nM). (B) Brain uptake of [^{11}C]SAR127303 can be blocked by JW642 (5 min pretreatment, i.v., 1 mg/kg), demonstrating specific MAGL binding of [^{11}C]SAR127303 in the brain. The unchanged uptake of [^{11}C]SAR127303 following pretreatment with JZL184 suggests limited brain uptake of JZL184.

irreversibility of [^{11}C]SAR127303 binding to MAGL (Figure 3B).

To test the ability of [^{11}C]SAR127303 as a tool for evaluation of MAGL inhibitors in the brain, we performed a study with 5 min pretreatment of two MAGL selective inhibitors, JZL184 and JW642. From our imaging results, JW642 showed good blockade in the brain, however, JZL184 did not, suggesting that JW642 has good brain permeability and MAGL inhibition, while JZL184 has limited brain uptake or poor MAGL engagement at this dose (Figure 4).

Our data in rodents support [^{11}C]SAR127303 as a new tool to visualize MAGL density in the living brain. The robust brain uptake of [^{11}C]SAR127303 potentially offers a method for quantification of MAGL density in inflammation-associated brain disorders, such as neurodegenerative diseases and mood disorders. We also anticipate utility of [^{11}C]SAR127303 for in vivo evaluation of target engagement of novel therapeutics early in compound development pipeline.

CONCLUSION

In summary, [^{11}C]SAR127303 binds to MAGL with high selectivity and specificity and provides a potential tool for quantitative imaging of MAGL density in the brain of living subjects. We are progressing [^{11}C]SAR127303 forward for evaluation as a novel MAGL PET radiotracer in nonhuman primates and humans.

METHODS

General Methods and Materials. Compound **3** and SAR127303 were prepared form SAI Life Sciences Ltd., Telangana, India. JZL184 and JW642 were purchased from Tocris Bioscience. Minneapolis, MN. All other reagents and solvents were of ACS-grade purity or higher and used without further purification. NMR data were recorded on a Varian 400 MHz magnet and were reported in ppm units downfield from trimethylsilane. Analytical separation was conducted on an Agilent 1100 series HPLC fit with a diode-array detector, quaternary pump, vacuum degasser, and autosampler. Mass spectrometry data were recorded on an Agilent 6310 ion trap mass spectrometer (ESI source) connected to an Agilent 1200 series HPLC equipped with a quaternary pump, vacuum degasser, diode-array detector, and an autosampler. [^{11}C]CO_2 (1.2 Ci) was obtained via the ^{14}N (p, α) ^{11}C reaction with nitrogen in the presence of 2.5% oxygen, with 11 MeV protons (Siemens Eclipse cyclotron), and trapped on molecular sieves in a TRACERlab FX-MeI synthesizer (General Electric).

All animal studies were carried out at Massachusetts General Hospital (PHS Assurance of Compliance No. A3596-01). The Subcommittee on Research Animal Care (SRAC) serves as the Institutional Animal Care and Use Committee (IACUC) for the Massachusetts General Hospital (MGH). SRAC reviewed and approved all procedures detailed in this paper.

PET/CT imaging was performed in anesthetized (isoflurane) Sprague−Dawley rats. Highly trained animal technicians monitored animal safety throughout all procedures and veterinary staff were responsible for daily care. All animals were socially housed in cages appropriate for the physical and behavioral health of the animals. Animals were given unlimited access to food and water.

Chemical Synthesis. *4-Chloro-N-(piperidin-4-ylmethyl)-benzenesulfonamide (**3**).* 4-Chlorobenzenesulfonyl chloride (**1**) (0.84 g, 4 mmol) and *tert*-butyl 4-(aminomethyl)piperidine-1-carboxylate (**2**) (0.85 g, 4 mmol) were added to a chilled solution (0 °C, ice water bath) in the presence of diisopropylethyl amine (DIPEA) (0.78 g, 6 mmol) and 4-dimethylaminopyridine (DMAP) (0.049 g, 0.4 mmol) in dichloromethane (DCM) (15 mL). After 16 h, the solvent was removed under vacuum and the residue partitioned between DCM and water (20 mL each). The organic layer was washed with brine (20 mL), dried with Na_2SO_4, filtered, and the solvent was removed under vacuum. Crude products were purified by flash chromatography. Pure fractions were combined, the solvent removed, and solids were collected (1.12 g, yield 72%). ^{1}H NMR (400 MHz, $CDCl_3$): δ 7.80 (d, J = 8.4 Hz, 2H), 7.51 (d, J = 8.4 Hz, 2H), 4.59−4.62 (m, 1H), 4.11 (s, 2H), 2.83−2.86 (m, 2H), 2.62−2.65 (m, 2H), 1.58−1.67 (m, 2H), 1.45 (s, 9H), 1.02−1.27 (m, 2H). The product from the previous step (1.1 g, 2.8 mmol) was dissolved in DCM chilled over an ice water bath (0 °C). TFA (3.2 g, 28 mmol) was added and stirred for 16 h. The solvent was removed under vacuum, and the residue partitioned between DCM and sodium bicarbonate solution (20 mL each). The organic layer was washed with brine (20 mL), dried (Na_2SO_4), filtered, and the solvent was removed under vacuum. Crude products were purified by flash chromatography. Pure fractions were combined, the solvent removed, and the product (**3**) was collected (0.7 g, yield 85%). ^{1}H NMR (400 MHz, $CDCl_3$): δ 7.80 (d, J = 8.4 Hz, 2H), 7.50 (d, J = 8.4 Hz, 2H), 4.62 (s, 1H), 3.05 (d, J = 12 Hz, 2H), 2.83 (d, J = 9.6 Hz, 2H), 2.51−2.57 (m, 2H), 1.57−1.66 (m, 2H), 1.02−1.10 (m, 2H). LC-MS calculated for $C_{12}H_{17}ClN_2O_2S$ [M]: 288.1; found [M + H]$^+$: 289.1.

1,1,1,3,3,3-Hexafluoropropan-2-yl 4-(((4-chlorophenyl)-sulfonamido)methyl)piperidine-1-carboxylate (SAR127303). HFIP (**4**) (0.17 g, 1 mmol) was added to a chilled solution (0 °C, ice water bath) of 4-nitrophenyl carbonochloridate (**5**) (0.4 g, 2 mmol), pyridine (0.16 g, 2 mmol), and DMAP (0.006 g, 0.05 mmol) in DCM (3 mL). After 16 h, a solution of **3** (0.3 g, 1 mmol) and DIPEA (0.33 g, 2.5 mmol) in DCM (15 mL) was added dropwise, and after 30 min the solvent was removed under vacuum and the residue partitioned between DCM and water (20 mL each). The organic layer was washed with brine (20 mL), dried (Na_2SO_4), and filtered, and the solvent was removed under vacuum. Crude products were purified by flash chromatography. Pure fractions were combined, the solvent removed, and solids were precipitated from pentane. The final product (SAR127303) was collected (0.06 g, yield 8%). Purity of SAR127303 was >99% as measured by HPLC. ^{1}H NMR (400 MHz, $CDCl_3$): δ 7.80 (d, J = 8.0 Hz, 2H), 7.52 (d, J = 8.4 Hz, 2H), 5.71−5.76 (m, 1H), 4.51−4.55 (m, 1H), 4.14−4.21 (m, 2H), 2.81−2.93 (m, 4H), 1.71−1.80 (m, 2H), 1.12−1.18 (m, 2H). LC-MS calculated for $C_{16}H_{17}ClF_6N_2O_4S$ [M]: 482.0; found [M − H]$^+$: 480.7.

DOI: 10.1021/acschemneuro.5b00293
ACS Chem. Neurosci. 2016, 7, 484−489

Radiosynthesis of [^{11}C]SAR127303. A conical vial (1 mL) sealed with a Teflon-lined silicone septum was purged with N_2 (15 mL/min for 5 min) 10 min prior to the end-of-bombardment and then charged with a solution of **3** (1 mg) and BEMP (7 μL) in anhydrous CH_3CN (100 μL). Carbon-11 labeled CO_2 was dispensed in a stream of nitrogen (15 mL/min) into the conical vial until radioactivity peaked. One minute later, a solution of $POCl_3$ (0.3 μL) in CH_3CN (100 μL) was added followed 1 min later by a CH_3CN solution (100 μL) of HFIP (1.5 μL). After 1 min, the reaction was quenched with water (700 μL) and purified on a reverse phase semipreparative HPLC (Agilent Eclipse XDB-18 column, 5 μm, 9.4 × 250 mm, 5.0 mL/min, 35% H_2O + 0.1% TFA/65% CH_3CN + 0.1% TFA, 254 nm) and the desired fraction was collected. The final product was diluted with 20 mL water and reformulated by loading onto a solid-phase exchange (SPE) C-18 cartridge, rinsing with water (5 mL), eluting with EtOH (1 mL), and diluting with saline (9 mL). The chemical and radiochemical purity of the final product was tested by analytical HPLC (Agilent Eclipse XDB-C18, 150 mm × 4.6 mm). The identity of the product was confirmed by analytical HPLC via coinjection with a SAR127303 reference standard. Specific activity of [^{11}C]SAR127303 (at time of injection): 1.6−2.3 mCi/nmol.

Log *D* Determination. An aliquot (~50 μL) of the formulated radiotracer was added to a test tube containing 2.5 mL of octanol and 2.5 mL of phosphate buffer solution (pH 7.4).The test tube was mixed by vortex for 2 min and then centrifuged for 2 min to fully separate the aqueous and organic phase. A sample taken from the octanol layer (0.1 mL) and the aqueous layer (1.0 mL) was saved for radioactivity measurement. An additional aliquot of the octanol layer (2.0 mL) was carefully transferred to a new test tube containing 0.5 mL of octanol and 2.5 mL of phosphate buffer solution (pH 7.4). The previous procedure (vortex mixing, centrifugation, sampling, and transfer to the next test tube) was repeated until six sets of aliquot samples had been prepared. The radioactivity of each sample was measured in a well counter (PerkinElmer, Waltham, MA).The log D of each set of samples was derived by the following equation: $\log D$ = log(decay corrected radioactivity in octanol sample × 10/decay-corrected radioactivity in phosphate buffer sample).

Rodent PET/CT Acquisition and Post Processing. Male Sprague−Dawley rats were utilized in pairs, anesthetized with inhalational isoflurane at 3% in a carrier of 1.5 L/min medical oxygen, and maintained at 2% isoflurane for the duration of the scan. The rats were arranged side-by-side in a Triumph Trimodality PET/CT/SPECT scanner (Gamma Medica, Northridge, CA). Rats were injected with unlabeled SAR127303 or vehicle via a lateral tail vein catheterized at the start of PET acquisition. Dynamic PET acquisition lasted for 60 min and was followed by computed tomography (CT) for anatomic coregistration and PET attenuation correction. PET data were reconstructed using a 3D-MLEM method resulting in a full width at half-maximum resolution of 1 mm. Reconstructed images were exported from the scanner in DICOM format along with an anatomic CT for rodent studies. These files were imported to PMOD (PMOD Technologies, Ltd.) and manually coregistered using six degrees of freedom.

Rodent PET/CT Image Analysis. Volumes of interest (VOIs) were drawn manually as spheres in brain regions guided by high resolution CT structural images and summed PET data, with a radius no less than 1 mm to minimize partial volume effects. Time−activity curves (TACs) were exported as decay-corrected activity per unit volume. The TACs were expressed as percent injected dose per unit volume for analysis.

AUTHOR INFORMATION

Corresponding Author

*Mailing address: Athinoula A. Martinos Center for Biomedical Imaging Massachusetts General Hospital, CNY 149, Room 5.022A, 149 13th Street, Charlestown, MA 02179. Phone: 617-724-9390. E-mail: cwang15@mgh.harvard.edu.

Author Contributions

C.W. discovered, synthesized, and purified [^{11}C]SAR127303. C.W. and J.M.H. planned experiments and performed data analysis. C.W., M.S.P., G.C.V.d.B., and F.A.S. performed the experiments. The manuscript was written through contributions of all the authors. All authors have given approval to the final version of the manuscript.

Funding

This research was supported by the Harvard/MGH Nuclear Medicine Training Program from the Department of Energy under Grant DE-SC0008430 (C.W. and G.C.V.d.B.) and NIH-NIDA T32 postdoctoral fellowship T32DA015036 (M.S.P.). This research was carried out at the Athinoula A. Martinos Center for Biomedical Imaging at the Massachusetts General Hospital, using resources provided by the Center for Functional Neuroimaging Technologies, P41EB015896, a P41 Regional Resource supported by the National Institute of Biomedical Imaging and Bioengineering (NIBIB), National Institutes of Health. This work also involved the use of instrumentation supported by the NIH Shared Instrumentation Grant Program and/or High-End Instrumentation Grant Program; specifically, Grant Number: S10RR015728.

Notes

The authors declare no competing financial interest.

ACKNOWLEDGMENTS

The authors are grateful to the Martinos Center radiopharmacy staff (Judit Sore, Kari Phan, Garima Gautam, and Samantha To) for help with radiotracer production. The authors are grateful to Dr. Aijun Zhu for assisting the rodent PET-CT studies.

ABBREVIATIONS

MAGL, monoacylglycerol lipase; PET, positron emission tomography; CT, computed tomography; EOS, end of synthesis; RCY, radiochemical yield; VOI, volume of interest; TAC, time−activity curve; BEMP, 2-*tert*-butylimino-2-diethylamino-1,3-dimethylperhydro-1,3,2-diazaphosphorine; HFIP, hexafluoroisopropanol; tPSA, total polar surface area; FAAH, fatty acid amide hydrolase; ABHD6, α/β-hydrolase 6; TFA, trifluoroacetic acid; SPECT, single-photon emission computed tomography; SPE, solid-phase exchange; DIPEA, diisopropylethyl amine; DCM, dichloromethane; DMAP, 4-dimethylaminopyridine; LPS, lipopolysaccharide; AA, arachidonic acid; AEA, *N*-arachidonoylethanolamine; CNS, central nervous system; PNS, peripheral nervous system; EOB, end of bombardment

REFERENCES

(1) Mulvihill, M. M., and Nomura, D. K. (2013) Therapeutic potential of monoacylglycerol lipase inhibitors. *Life Sci. 92* (8−9), 492−7.

(2) Ahn, K., McKinney, M. K., and Cravatt, B. F. (2008) Enzymatic pathways that regulate endocannabinoid signaling in the nervous system. *Chem. Rev. 108* (5), 1687−707.

(3) Long, J. Z., and Cravatt, B. F. (2011) The metabolic serine hydrolases and their functions in mammalian physiology and disease. *Chem. Rev. 111* (10), 6022−63.

(4) Griebel, G., Pichat, P., Beeske, S., Leroy, T., Redon, N., Jacquet, A., Francon, D., Bert, L., Even, L., Lopez-Grancha, M., Tolstykh, T., Sun, F., Yu, Q., Brittain, S., Arlt, H., He, T., Zhang, B., Wiederschain, D., Bertrand, T., Houtmann, J., Rak, A., Vallee, F., Michot, N., Auge, F., Menet, V., Bergis, O. E., George, P., Avenet, P., Mikol, V., Didier,

DOI: 10.1021/acschemneuro.5b00293
ACS Chem. Neurosci. 2016, 7, 484−489

M., and Escoubet, J. (2015) Selective blockade of the hydrolysis of the endocannabinoid 2-arachidonoylglycerol impairs learning and memory performance while producing antinociceptive activity in rodents. *Sci. Rep. 5*, 7642.
(5) Pertwee, R. G. (2006) The pharmacology of cannabinoid receptors and their ligands: an overview. *Int. J. Obes. 30*, S13−8.
(6) Hohmann, A. G., and Suplita, R. L., 2nd (2006) Endocannabinoid mechanisms of pain modulation. *AAPS J. 8* (4), E693−708.
(7) Jhaveri, M. D., Richardson, D., and Chapman, V. (2007) Endocannabinoid metabolism and uptake: novel targets for neuropathic and inflammatory pain. *Br. J. Pharmacol. 152* (5), 624−32.
(8) Lambert, D. M. (2007) Allergic contact dermatitis and the endocannabinoid system: from mechanisms to skin care. *ChemMedChem 2* (12), 1701−2.
(9) Bisogno, T., and Di Marzo, V. (2007) Short- and long-term plasticity of the endocannabinoid system in neuropsychiatric and neurological disorders. *Pharmacol. Res. 56* (5), 428−42.
(10) Matias, I., and Di Marzo, V. (2007) Endocannabinoids and the control of energy balance. *Trends Endocrinol. Metab. 18* (1), 27−37.
(11) Pagotto, U., Marsicano, G., Cota, D., Lutz, B., and Pasquali, R. (2006) The emerging role of the endocannabinoid system in endocrine regulation and energy balance. *Endocr. Rev. 27* (1), 73−100.
(12) Bifulco, M., Laezza, C., Gazzerro, P., and Pentimalli, F. (2007) Endocannabinoids as emerging suppressors of angiogenesis and tumor invasion (review). *Oncol. Rep. 17* (4), 813−6.
(13) Long, J. Z., Li, W., Booker, L., Burston, J. J., Kinsey, S. G., Schlosburg, J. E., Pavon, F. J., Serrano, A. M., Selley, D. E., Parsons, L. H., Lichtman, A. H., and Cravatt, B. F. (2009) Selective blockade of 2-arachidonoylglycerol hydrolysis produces cannabinoid behavioral effects. *Nat. Chem. Biol. 5* (1), 37−44.
(14) Nomura, D. K., Morrison, B. E., Blankman, J. L., Long, J. Z., Kinsey, S. G., Marcondes, M. C., Ward, A. M., Hahn, Y. K., Lichtman, A. H., Conti, B., and Cravatt, B. F. (2011) Endocannabinoid hydrolysis generates brain prostaglandins that promote neuroinflammation. *Science 334* (6057), 809−13.
(15) Schlosburg, J. E., Blankman, J. L., Long, J. Z., Nomura, D. K., Pan, B., Kinsey, S. G., Nguyen, P. T., Ramesh, D., Booker, L., Burston, J. J., Thomas, E. A., Selley, D. E., Sim-Selley, L. J., Liu, Q. S., Lichtman, A. H., and Cravatt, B. F. (2010) Chronic monoacylglycerol lipase blockade causes functional antagonism of the endocannabinoid system. *Nat. Neurosci. 13* (9), 1113−9.
(16) Fowler, C. J. (2012) Monoacylglycerol lipase - a target for drug development? *Br. J. Pharmacol. 166* (5), 1568−85.
(17) King, A. R., Dotsey, E. Y., Lodola, A., Jung, K. M., Ghomian, A., Qiu, Y., Fu, J., Mor, M., and Piomelli, D. (2009) Discovery of potent and reversible monoacylglycerol lipase inhibitors. *Chem. Biol. 16* (10), 1045−52.
(18) Chang, J. W., Niphakis, M. J., Lum, K. M., Cognetta, A. B., 3rd, Wang, C., Matthews, M. L., Niessen, S., Buczynski, M. W., Parsons, L. H., and Cravatt, B. F. (2012) Highly selective inhibitors of monoacylglycerol lipase bearing a reactive group that is bioisosteric with endocannabinoid substrates. *Chem. Biol. 19* (5), 579−88.
(19) Alhouayek, M., Lambert, D. M., Delzenne, N. M., Cani, P. D., and Muccioli, G. G. (2011) Increasing endogenous 2-arachidonoylglycerol levels counteracts colitis and related systemic inflammation. *FASEB J. 25* (8), 2711−21.
(20) Hicks, J. W., Parkes, J., Tong, J., Houle, S., Vasdev, N., and Wilson, A. A. (2014) Radiosynthesis and ex vivo evaluation of [(11)C-carbonyl]carbamate- and urea-based monoacylglycerol lipase inhibitors. *Nucl. Med. Biol. 41* (8), 688−94.
(21) Saario, S. M., Savinainen, J. R., Laitinen, J. T., Jarvinen, T., and Niemi, R. (2004) Monoglyceride lipase-like enzymatic activity is responsible for hydrolysis of 2-arachidonoylglycerol in rat cerebellar membranes. *Biochem. Pharmacol. 67* (7), 1381−7.
(22) Savinainen, J. R., Saario, S. M., and Laitinen, J. T. (2012) The serine hydrolases MAGL, ABHD6 and ABHD12 as guardians of 2-arachidonoylglycerol signalling through cannabinoid receptors. *Acta Physiol. 204* (2), 267−76.
(23) Saario, S. M., Salo, O. M., Nevalainen, T., Poso, A., Laitinen, J. T., Jarvinen, T., and Niemi, R. (2005) Characterization of the sulfhydryl-sensitive site in the enzyme responsible for hydrolysis of 2-arachidonoyl-glycerol in rat cerebellar membranes. *Chem. Biol. 12* (6), 649−56.
(24) Long, J. Z., Nomura, D. K., and Cravatt, B. F. (2009) Characterization of monoacylglycerol lipase inhibition reveals differences in central and peripheral endocannabinoid metabolism. *Chem. Biol. 16* (7), 744−53.
(25) Hooker, J. M., Reibel, A. T., Hill, S. M., Schueller, M. J., and Fowler, J. S. (2009) One-pot, direct incorporation of [11C]CO2 into carbamates. *Angew. Chem., Int. Ed. 48* (19), 3482−5.
(26) Rusjan, P. M., Wilson, A. A., Mizrahi, R., Boileau, I., Chavez, S. E., Lobaugh, N. J., Kish, S. J., Houle, S., and Tong, J. (2013) Mapping human brain fatty acid amide hydrolase activity with PET. *J. Cereb. Blood Flow Metab. 33* (3), 407−14.

DOI: 10.1021/acschemneuro.5b00293
ACS Chem. Neurosci. 2016, 7, 484−489